7-28-2014

Size-dependent vibronic coupling in α-Fe2O3

Kenneth Robert O'Neal
koneal5@vols.utk.edu

J M. Patete
State University of New York at Stony Brook

P Chen
University of Tennessee, Knoxville

Brian S. Holinsworth
University of Tennessee, Knoxville

J M. Smith
State University of New York at Stony Brook

See next page for additional authors

Size-Dependent Vibronic Coupling in α-Fe_2O_3

K. R. O'Neal,[1] J. M. Patete,[2] P. Chen,[1] B. S. Holinsworth,[1] J. M. Smith,[2] N. Lee,[3] S. -W. Cheong,[4] S. S. Wong,[2,5] C. Marques,[6] M. C. Aronson,[5,6] and J. L. Musfeldt[1]

[1]*Department of Chemistry, University of Tennessee, Knoxville, Tennessee 37996, USA*

[2]*Department of Chemistry, State University of New York at Stony Brook, Stony Brook, New York 11794-3400, USA*

[3]*Department of Physics and IPAP, Yonsei University, Seoul 120-749, Republic of Korea*

[4]*Rutgers Center for Emergent Materials and Department of Physics and Astronomy, Rutgers University, Piscataway, New Jersey 08854, USA*

[5]*Condensed Matter Physics and Materials Science Department, Brookhaven National Laboratory, Upton, New York 11973, USA*

[6]*Department of Physics and Astronomy, Stony Brook University, Stony Brook, New York 11794-3800, USA*

(Dated: December 9, 2019)

Abstract

We report the discovery of finite length scale effects on vibronic coupling in nanoscale α-Fe_2O_3 as measured by the behavior of vibronically-activated *d-d* on-site excitations of Fe^{3+} as a function of size and shape. An oscillator strength analysis reveals that the frequency of the coupled symmetry-breaking phonon changes with size, a crossover that we analyze in terms of increasing three-dimensional character to the displacement pattern. These findings demonstrate the flexibility of mixing processes in confined systems and suggest a strategy for both enhancing and controlling charge-lattice interactions in other materials.

KEYWORDS: hematite nanoparticles, vibronic coupling, color band analysis, finite length scale effects

INTRODUCTION

Charge-lattice coupling is one of the most celebrated interactions in functional materials. The mechanism underlies a wide variety of scientifically and technologically important processes including superconductivity, charge density wave formation, vibronic coupling, and photochemical reactions, just to name a few [1–9]. Each expresses itself in different ways. One example of vibronic coupling is the activation of *d*-manifold excitations in transition metal-containing materials [10–12]. These excitations probe the crystal field environment and are often called color bands when they appear in the visible range. Vibronic coupling in which an odd parity phonon interacts with an on-site *d*-*d* excitation to break inversion symmetry has been investigated in a number of bulk oxides like $CuGeO_3$, $LiNbO_3$, and $BiFeO_3$ [13–15]. By contrast, the mechanism is relatively unexplored in nanoscale materials [16–18]. α-Fe_2O_3, commonly known as hematite [19–22], attracted our attention as a system with which to reach beyond temperature, magnetic field, and pressure tuning of color band activation [23–25] to investigate size and shape effects.

In this paper, we report the discovery of finite length scale effects on vibronic coupling in α-Fe_2O_3, and a crossover in the coupling phonon frequency (from the 530 cm^{-1} phonon mode in the single crystal to the 470 cm^{-1} mode in the smallest nanoparticles) that is driven by a change in the dimensionality of the displacement pattern. Analysis reveals that the mode character becomes more three-dimensional with decreasing size. We confirm these findings and uncover a two-state mixing process at intermediate sizes via direct vibrational property measurements and comparison with prior lattice dynamics calculations [26]. Similar flexibility in charge-lattice energy transfer processes may underpin the remarkable properties of other confined systems [27–31]. These findings advance the fundamental understanding of vibronic coupling and functionality in iron-containing solids [32–36], present a strategy for controlling charge-lattice interactions, and are relevant to more complicated energy transfer processes in which size acts as a tuning parameter. Examples include direct vs. indirect band gap crossover and catalytic activity [28, 37].

METHODS

Various sizes and shapes of α-Fe_2O_3 nanoparticles were prepared by hydrothermal methods (Table I) and their magnetic and structural properties characterized [38–41]. For comparison, a high quality single crystal was grown by flux techniques [24], and bulk powder was purchased from Alfa Aeser (99.999%). The nanoparticles and bulk powder were mixed with a matrix and pressed into pellets for optical transmittance measurements (30 - 700, and 8700 - 17000 cm^{-1}). Absorption was calculated as $\alpha(\omega) = (1/hd)\ln(T(\omega))$, where $T(\omega)$ is the measured transmittance, h is the sample loading, and d is thickness. Variable temperature measurements from 4 to 300 K were performed with the use of an open flow helium cryostat. Oscillator strength was calculated as $f = \frac{2c}{N_e \pi \omega_\rho^2} \int_{\omega 1}^{\omega 2} n\alpha(\omega) d\omega$, where $N_e = 5$ is the number of electrons per Fe site, n $\simeq$ 2.23 is the refractive index, ω_ρ is the plasma frequency $\omega_\rho \equiv \sqrt{\frac{e^2 \rho}{m\epsilon_0}}$, e and m are the charge and mass of an electron, ϵ_0 is the vacuum dielectric constant, ρ is the density of Fe sites, c is the speed of light, and ω_1 and ω_2 are the frequency limits of integration [42]. Since the $^6A_{1g} \rightarrow {}^4T_{1g}$ Fe^{3+} on-site excitation that is our focus here overlaps with the next higher energy d-d transition, a simple integration could not be used. Instead, a Gaussian fit to the spectral band was used to determine oscillator strength. This fitting procedure reduces error in oscillator strength trends originating from different temperature dependencies of the two electronic excitations.

RESULTS AND DISCUSSION

Figure 1 (a-c) displays the absorption spectra for single crystalline hematite and select nanoparticles at 4 and 300 K. The dominant structure in this spectral region is assigned as the $^6A_{1g} \rightarrow {}^4T_{1g}$ Fe^{3+} on-site electronic excitation [10]. This d-d excitation and the one around 16,000 cm^{-1} (not shown) are formally spin and parity forbidden, but are observed due to exchange interactions, spin-orbit coupling, and odd parity phonons that break inversion symmetry [10–12]. The low temperature single crystal spectrum reveals excitons and a magnon sideband on the leading edge of the d-d transition [24]. While the magnon sideband is still observed in the nanoparticle spectra, the excitons are more obscured, probably due to the random orientation of the nanoparticles combined with the directional character and low oscillator strengths of the excitons. We calculated the oscillator strength of the electronic

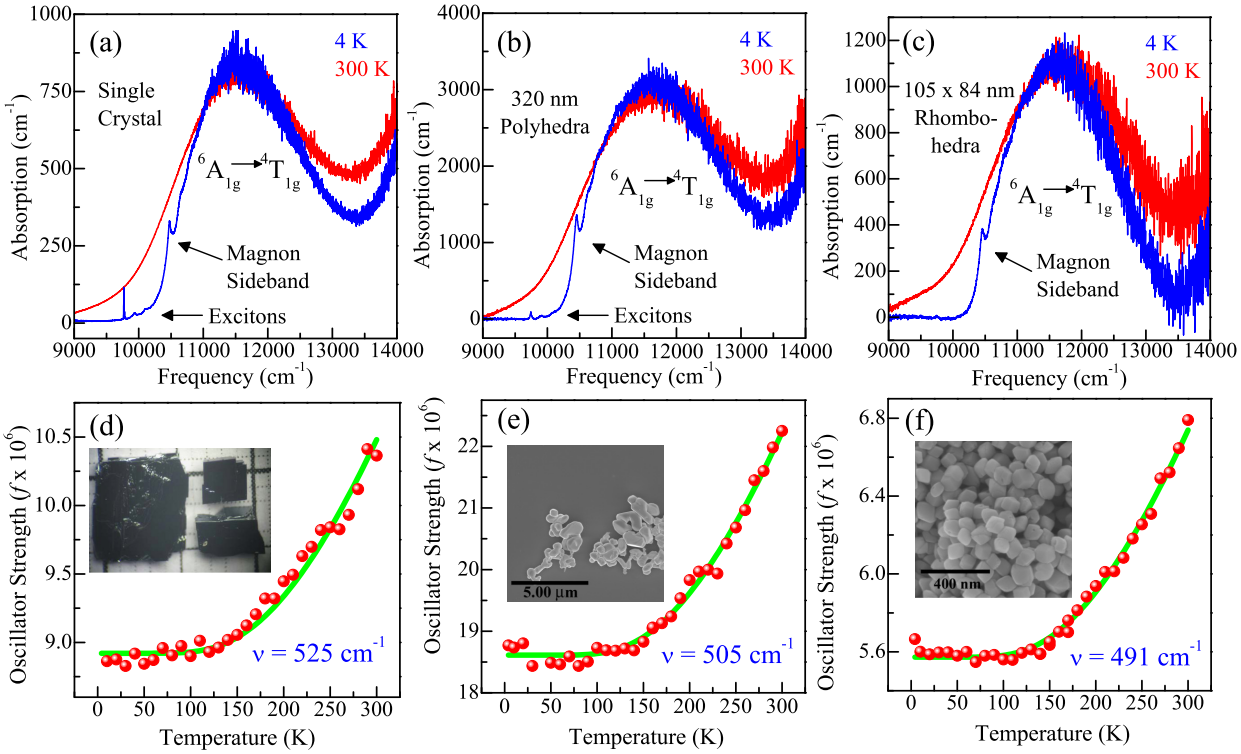

FIG. 1. (a-c) Absorption at 4 and 300 K for the (111) plane of the single crystal, nanopolyhedra, and largest nanorhombohedra, respectively. Excitons and a magnon sideband can be seen in the low temperature spectrum of the single crystal, whereas the nanoparticles reveal strong magnon sideband excitations but only weak exciton features. (d-f) Oscillator strength of the color band transition as a function of temperature for the single crystal, nanopolyhedra, and largest nanorhombohedra, respectively. The green line represents a fit to the vibronic coupling model described in the text. Insets: Images of each material.

excitation over the full temperature range (Figure 1 (d-f)). The 260 K discontinuity in the oscillator strength of the single crystal is a signature of the spin-flop transition [43]. Magnetization measurements show that the spin-flop is present in the nanoparticles but is obscured by the error bars on oscillator strength [41].

The temperature dependent oscillator strength for a vibronically activated excitation is described as

$$f = f_0 \coth(h\nu/2kT), \tag{1}$$

where f is oscillator strength, f_0 is the limiting low temperature oscillator strength, ν is

the frequency of the vibrational mode that activates the on-site excitation, h is Planck's constant, k is Boltzmann's constant, and T is temperature [12]. We employed this model to fit the oscillator strength trends and extract the coupling phonon frequencies. The best fits are shown in Figure 1 (d-f), and the fit parameters are summarized in Table I. The magnitude of the oscillator strength of the *d-d* excitation in each sample agrees well with typical oscillator strengths of parity forbidden transitions observed in other transition metal oxides like $CuGeO_3$ [13] and iron containing materials such as $CsFeCl_3$ [44]. Our extracted value of ν=525 cm^{-1} for single crystalline hematite is significantly larger than the previously reported 139 cm^{-1} acoustic phonon [23], but lies within the range of phonons energies in hematite. In fact, it is an excellent match for the E_u symmetry mode centered at 520 cm^{-1} [45]. This difference likely arises from the fact that the previous authors measured only along one crystal axis, did not investigate below 100 K, and used an approximate model that assumes that both the ground and excited state are characterized by harmonic oscillators that share force constants and equilibrium positions [46, 47]. Our more comprehensive analysis was also carried out on a micron-sized bulk powder (in order to compare the single crystal to the randomly oriented nanoparticles), nanocubes, nanopolyhedra, nanorice, and four sizes of nanorhombohedra. Figure 1 shows some representative examples. The nanoparticle dimensions and extracted parameters are summarized in Table I.

Figure 2 displays the coupling phonon frequency, ν, that we extract from this vibronic coupling analysis, versus average particle size. There is excellent agreement between the two largest sizes (the single crystal and micron-sized bulk powder). Both yield a coupling phonon frequency of about ν=525 cm^{-1}. For the 450 nm nanocubes, we extract a coupling frequency of 507 cm^{-1}. For the smallest size of nanorhombohedra, we find ν=469 cm^{-1}. Overall, reduction of particle size decreases the coupling phonon frequency that activates the color band excitation. This decrease is much larger than what might be expected from size-dependent changes in phonon frequencies for hematite alone [49].

In order to activate the spin and parity forbidden on-site excitation, the coupling phonon mode must break the inversion symmetry around the Fe^{3+} center. The activating phonon must then be of ungerade symmetry, i.e. infrared active. To test whether the phonon frequencies extracted from our vibronic coupling analysis correlate with actual vibrational modes, we measured the infrared response of each set of nanoparticles (Figure 3 a). From our vibronic coupling analysis, we extract ν=525 cm^{-1} for the bulk material, and in the

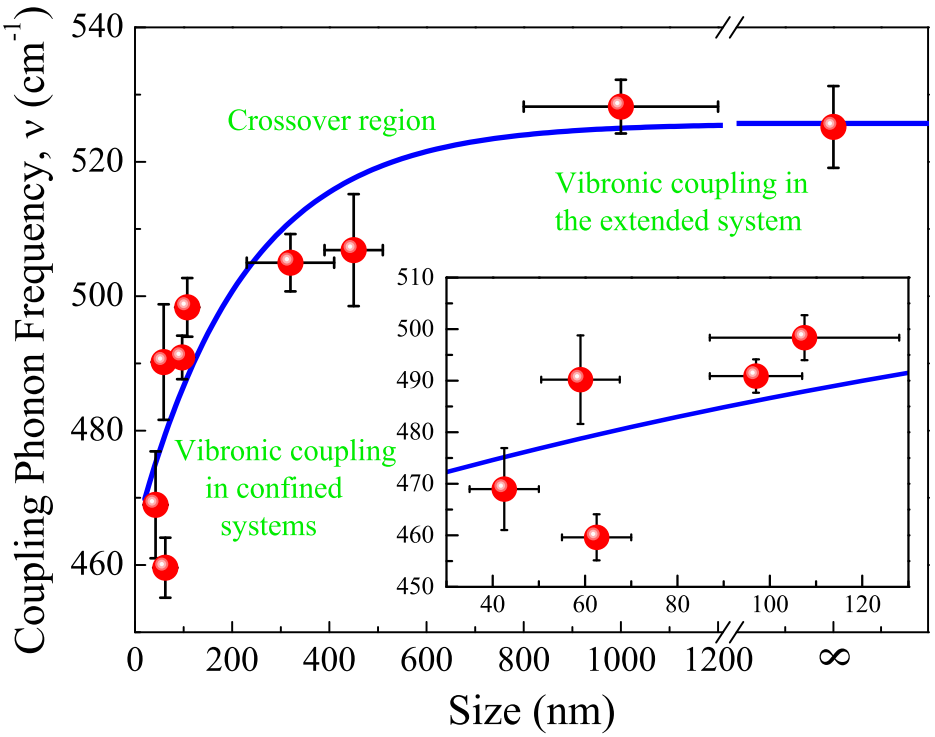

FIG. 2. Coupling phonon frequency, ν, versus average particle size as determined by the oscillator strength analysis described in the text. The blue line guides the eye. Interestingly, this trend depends only on the particle size, with shape playing no role. Inset: Expanded view of the trend for the smallest nanoparticles.

infrared there is an E_u symmetry phonon mode observed at 530 cm^{-1} [50]. This phonon mode consists mainly of atomic displacements within the *ab* plane [26]. For the 450 nm cubes, ν is found to be 507 cm^{-1}, which is now between the peaks observed at 560 cm^{-1} and 480 cm^{-1}, indicating that both modes are contributing to the activation of the color band. Turning to the smallest nanoparticles (the 35 x 50 nm rhombohedra), ν is determined to be 469 cm^{-1}. Indeed, the infrared spectrum does reveal a phonon mode at 470 cm^{-1}. The displacement pattern for this mode consists of combined *ab* plane and *c* axis motion [26]. Taken together, these findings suggest that there is a crossover from the 530 cm^{-1} phonon mode activating the transition at large sizes to the 470 cm^{-1} mode at small sizes. In the intermediate size region, our analysis yields a weighted average of the two mode frequencies (530 and 470 cm^{-1}) [51]. This size driven crossover is reminiscent of a simple two state kinetics model, with particle size in place of time, and the concentrations (or two states in our case) are the relative contribution of the 530 and 470 cm^{-1} phonon modes to ν.

TABLE I. Summary of the material characteristics and fitting parameters obtained from the vibronic coupling model described in the text demonstrating how ν decreases with particle size, regardless of shape. Error bars in size represent a distribution of sizes.

Sample	Length (nm)	Width (nm)	f_0 (10^{-6})	ν (cm^{-1})
single crystal	42 μm	-	10.8	525 ± 6
bulk powder	1000 nm	-	4.73	529 ± 4
cubes	450 ± 60	450 ± 60	25.1	507 ± 8
polyhedra	320 ± 90	320 ± 90	18.6	505 ± 4
rice	148 ± 32	67 ± 10	1.61	498 ± 4
rhombohedra	105 ± 16	84 ± 12	5.57	491 ± 3
rhombohedra	75 ± 8	50 ± 7	5.38	460 ± 4
rhombohedra	59 ± 9	59 ± 8	1.97	490 ± 9
rhombohedra	50 ± 8	35 ± 7	2.54	469 ± 8

To understand why this crossover occurs, we must consider how nanoscale confinement affects the structure of hematite. As particle size decreases, the hematite unit cell expands anisotropically, with the c axis expanding faster than the a-axis [52]. While this trend has been formally demonstrated for particle sizes below 63 nm [52], the argument can presumably be extended to the sizes discussed in our work. As the unit cell expands, c-directed displacements in the 470 cm^{-1} mode become more important. This enhanced symmetry breaking provides a mechanism for why the electronic transition crosses over to be activated by a lower frequency phonon mode at small size. Moreover, the trend appears to be independent of particle shape, as the nanorice (with a vastly different aspect ratio than the nanocubes and nanorhombohedra) and the multifacted polyhedra follow the same trend with excellent agreement. The reduction of ν also suggests that small nanoparticles should be more sensitive to temperature than bulk hematite as indicated by the greater relative increase in oscillator strength [41].

At low temperature, coupling between the activating phonon mode and the electronic transition is reduced, and the activating phonon mode may recover some oscillator strength [53]. We carried out variable temperature infrared measurements to test this idea. Figure 3 (b,c) displays the 4 and 300 K infrared absorption spectra for the nanocubes and largest

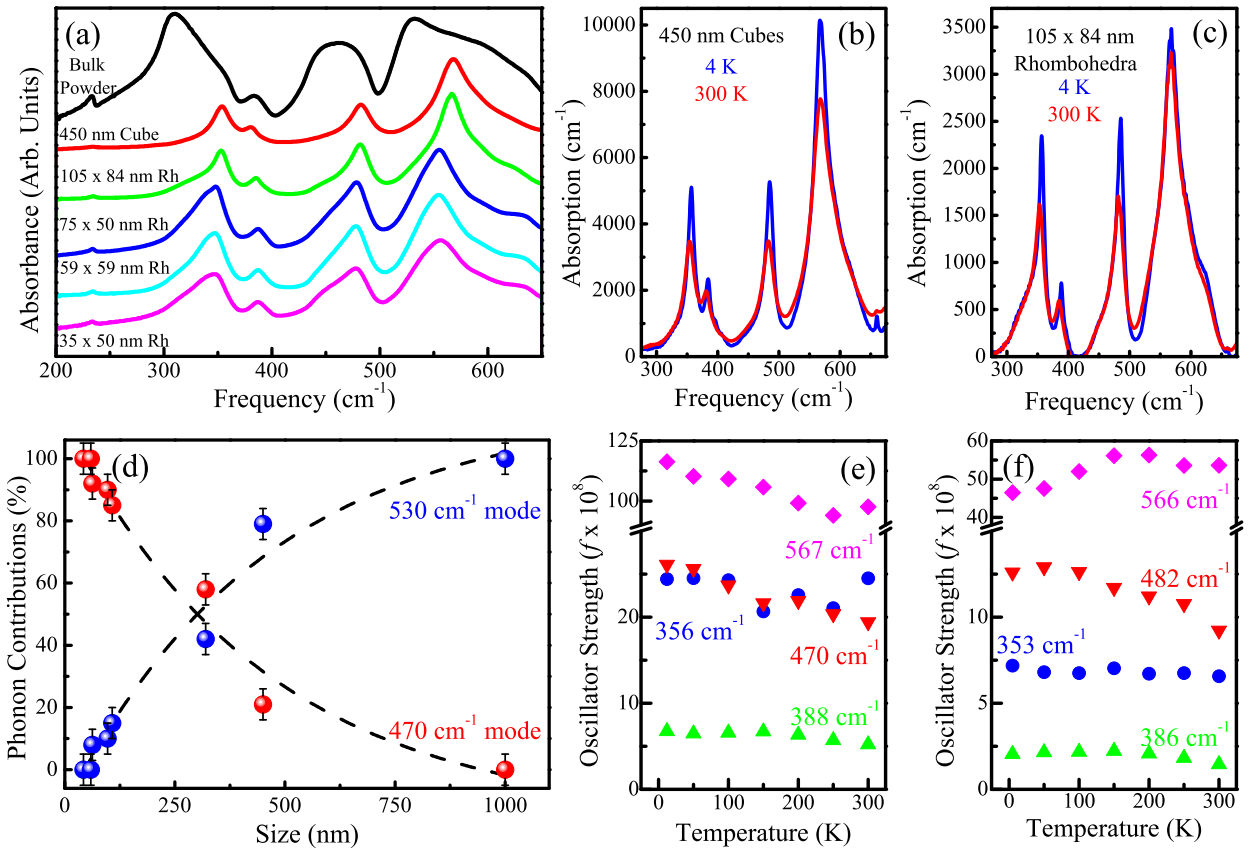

FIG. 3. (a) Representative 300 K infrared absorption spectra for the bulk powder (black), nanocubes (red), and nanorhombohedra from largest (green) to smallest (magenta). Infrared response at 4 and 300 K for the (b) 450 nm nanocubes, and (c) 84 nm nanorhombohedra. All phonon modes harder upon cooling. (d) Contribution of the 470 and 530 cm^{-1} phonon modes to the activation of the on-site excitation. At large sizes, the 530 cm^{-1} mode consisting of only *ab* plane motion dominates. There is a strong superposition at intermediate sizes as well as a crossover. At small sizes, the 470 cm^{-1} mode consisting of *ab* plane and *c* axis motion dominates. Analysis of the data in (b) and (c) allow us to follow phonon oscillator strengths as a function of temperature. Panels (e) and (f) show our findings for the nanocubes and nanorhombohedra, respectively. Only the phonon modes extracted from our vibronic coupling analysis gain significant oscillator strength at low temperature, a finding that directly confirms the aforementioned weighting crossover in the intermediate size regime.

size of rhombohedra, respectively. Again, due to the overlapping spectral features a simple integration could not be performed, and a standard peak fit method was used to determine the oscillator strength of each mode. In the nanocubes, both the 560 and 470 cm^{-1} phonon modes show a modest increase in oscillator strength at low temperature while the oscillator strength of the other phonon modes remain constant. This indicates that both modes are coupled to the electronic transition, as predicted by our vibronic coupling analysis. In the largest size of rhombohedral nanoparticles, the 480 cm^{-1} E_u phonon mode regains oscillator strength at low temperature while the 560 cm^{-1} mode remains constant. This nicely confirms that only the 480 cm^{-1} phonon mode is coupled to the electronic transition as anticipated (Figure 3 (e,f)).

CONCLUSION

In summary, we investigated the optical properties of α-Fe_2O_3 as a function of size, shape, and temperature and compared our results with micron-sized bulk powder and single crystals. We find that the vibronically-activated *d-d* on-site excitation of Fe^{3+} in the single crystal is activated by the 530 cm^{-1} phonon mode consisting of *ab* plane motion rather than a 139 cm^{-1} acoustic phonon as previously reported [23]. Moreover, as particle size is reduced, the frequency of the vibronically coupled phonon that allows the transition decreases and crosses over to the 470 cm^{-1} vibrational mode (which contains both *ab* plane and *c*-directed motion) at the smallest size. This universal size dependence stems from an anisotropic expansion of the unit cell leads to a more three dimensional type of symmetry breaking courtesy of the 470 cm^{-1} phonon. This trend is confirmed by an increase in oscillator strength of the vibronically coupled phonon modes at low temperature. The discovery of size-dependent vibronic coupling broadens our understanding of finite length scale effects in transition metal oxides. This effect may be present in other transition metal containing materials such as $CuGeO_3$ or $CsFeCl_3$ [13, 44], where nanoscale confinement enhances functionality.

ACKNOWLEDGMENTS

This research is supported by the Materials Science Division, Office of Basic Energy Sciences, U.S. Department of Energy under Awards DE-FG02-01ER45885 (JLM, spectroscopy), DE-AC02-98CH10886 (SSW, nanoparticle growth and characterization), and DE-AC02-98CH1886 (MCA, magnetic properties). Work at Rutgers University is supported by the NSF under Grant No. NSFDMR-1104484 (SWC, single crystal growth). We thank T. V. Brinzari for useful discussions.

[1] J. Bardeen, L. N. Cooper, and J. R. Schrieffer, Phys. Rev. **106**, 162 (1957).

[2] N. Driza, S. Blanco-Canosa, M. Bakr, S. Soltan, M. Jhalid, L. Mustafa, J. Jawashima, G. Christianai, J. -U. Habermeier, G. Khaliullin, C. Ulrich, M. LeTacon, and B. Keimer, Nature Mater. **11**, 675 (2012).

[3] D. C. Johnston, Adv. Phys. **59**, 803 (2010).

[4] G. Grüner, Rev. Mod. Phys. **60**, 1129 (1988).

[5] J. Michl, and J. Bonacic-Koutecky, *Electronic Aspects of Organic Photochemistry* (Wiley, New York, 1990).

[6] R. G. Mckinlay, J. M. Źurek, and M. J. Paterson, Adv. Inorg. Chem. **62**, 351 (2010).

[7] V. Coropceanu, J. Cornil, C. Jérôme, D. A. S. Filho, Y. Olivier, R. Silbey, and J.-L. Brédas, Chem. Rev. **107**, 926 (2007).

[8] O. Tal, M. Krieger, B. Leerink, and J. M. van Ruitenbeek, Phys. Rev. Lett. **100**, 196804 (2008).

[9] O. G. Holmes and D. S. McClure, J. Chem. Phys. **26**, 1686 (1957).

[10] D. D. Sell, R. L. Greene, and R. M. White, Phys. Rev. **158**, 489 (1967).

[11] L. R. Lohr Jr., Coord. Chem. Rev. **8**, 241 (1972).

[12] C. J. Ballhausen, *Ligand Field Theory*; (McGraw-Hill, New York, 1962).

[13] M. Bassi, P. Camagni, R. Rolli, G. Samoggia, F. Parmigiani, G. Dhalenne, and A. Revcolevschi, Phys. Rev. B **54**, R11030 (1996).

[14] E. Montoya, J. A. Sanz-García, and L. E. Bausa, Spec. Acta Part A **54**, 2081 (1998).

[15] X. S. Xu, T. V. Brinzari, S. Lee, Y. H. Chu, L. W. Martin, A. Kumar, S. McGill, R. C. Rai, R. Ramesh, V. Gopalan, S.-W. Cheong, and J. L. Musfeldt, Phys. Rev. B **79**, 134425 (2009).

[16] A. M. Kelley, ACS Nano **5**, 5254 (2011).

[17] P. H. de Oliveira Neto, J. F. Teixeira, W. F. da Cunha, R. Gargano, and G. M. e Silva, J. Phys. Chem. Lett. **3**, 3039 (2012).

[18] Q. Zhang, X. Liu, M. I. B. Utama, J. Zhang, M. de la Mata, J. Arbiol, Y. Lu, T. C. Sum, and Q. Xiong, Nano Lett. **12**, 6420 (2012).

[19] K. D. Finkelstein, Q. Shen, and S. Shastri, Phys. Rev. Lett. **69**, 1612 (1992).

[20] X.-G. Wang, W. Weiss, Sh. K. Shaikhutdinov, M. Ritter, M. Petersen, F. Wagner, R. Schlögl, and M. Scheffler, Phys. Rev. Lett. **81**, 1038 (1998).

[21] J. Chen, L. Xu, W. Li, X. Giou, Adv. Mater. **17**, 582 (2005).

[22] J. Lian, X. Duan, J. Ma, P. Peng, T. Kim, and W. Zheng, ACS Nano **3**, 3749 (2009).

[23] L. A. Marusak, R. Messier, and W. B. White, J. Phys. Chem. Solids **41**, 981 (1980).

[24] P. Chen, N. Lee, S. McGill, S.-W. Cheong, and J. L. Musfeldt, Phys. Rev. B **85**, 174413 (2012).

[25] T. Kawamura, S. Endo, M. Kobayashi, and S.-I. Narita, J. Phys. Soc. Japan **53**, 3684 (1984).

[26] K. Iishi, Phys. Chem. Miner. **3** 1 (1978).

[27] Y. Q. Zhu, T. Sekine, K. S. Brigatti, S. Firth, R. Tenne, R. Rosentsveig, H. W. Kroto, and D. R. M. Walton, J. Am. Chem. Soc. **125**, 1329 (2003).

[28] K. F. Mak, C. Lee, J. Hone, J. Shan, and T. F. Heinz, Phys. Rev. Lett. **105** 136805.

[29] Q.-C. Sun, L. Yadgarov, R. Rosentsveig, G. Seifert, R. Tenne, and J. L. Musfeldt, ACS Nano **7** 3506 (2012).

[30] S. Nakade, Y. Saito, W. Kubo, T. Kitamura, Y. Wada, and S. Yanagida, J. Phys. Chem. B **107**, 8607 (2003).

[31] Y. Jin, J. Wang, B. Sun, J. C. Blakesley, and N. C. Greenham, ACS Nano **8**, 1649 (2008).

[32] J. Wang, J. B. Neaton, H. Zheng, V. Nagarajan, S. B. Ogale, B. Liu, D. Viehland, V. Vaithyanathan, D. Schlom, U. V. Waghmare, N. A. Spaldin, K. M. Rabe, M. Wuttig, and R. Ramesh, Science **299**, 1719 (2003).

[33] Y. Kamihara, H. Hiramatsu, M. Hirano, R. Kawamura, H. Yanagi, T. Kamiya, and H. Hosono, J. Am. Chem. Soc. **128**, 10012 (2006).

[34] J. W. Geus, Appl. Cat. **25**, 331 (1986).

[35] X. Xu, J. Zhuang, and X. Wang, J. Am. Chem. Soc. **130** 12527 (2008).

[36] M. Atanasov, J. M. Zadrozny, J. R. Long, and F. Neese, Chem. Sci. **4**, 139 (2013).

[37] X. Zhou, W. Xu, G. Liu, D. Panda, and P. Chen, J. Am. Chem. Soc. **132**, 138 (2009).

[38] P. Zhifa, C. Minhua, Y. Jing, H. Kunlin, and H. Changwen, Nanotechnology **17**, 799 (2006).

[39] C.-J. Jia, L.-D. Sun, Z.-G. Yan, L.-P. You, F. Luo, X.-D. Han, Y.-C. Pang, Z. Zhang, and C.-H. Yan, Angew. Chem. Int. Ed. **44**, 4328 (2005).

[40] T.-J. Park and S. S. Wong, Chem. Mater. **18**, 5289 (2006).

[41] See Supplemental Material for more information.

[42] F. Wooten, *Optical Properties of Solids*; (Academic Press, New York, 1972).

[43] F. J. Morin, Phys. Rev. **78**, 819 (1950).

[44] T. Tsuboi, M. Chiba, and Y. Ajiro, Phys. Rev. B **32**, 354 (1985).

[45] A. U. Gehring and A. M. Hofmeister, Clay Clay Miner. **42**, 409 (1994).

[46] L. L. Lohr Jr., J. Chem. Phys. **50**, 4596 (1969).

[47] The previously published data are inconsistent with our data in two main ways. The first relates to the spectrum itself. The authors note that their oscillator strength is an order of magnitude higher than previous reports [48]. The spectra of Marusak *et al.* also display shoulders on either side of the electronic feature, which probably arise from sample impurities. The second difference relates to fitting the temperature dependent oscillator strength trend. The absence of data below 100 K results in large error bars in the value of f_0 which is critical for an accurate fit. The functional form used by the previous authors does not fit to the oscillator strengths that we obtained, so we elected to use the more common model described in the text.

[48] G. Lehmann and H. Harder, Am. Min. **55**, 98 (1970).

[49] I. V. Chernyshova, M. F. Hochella Jr., and A. S. Madden, Phys. Chem. Chem. Phys. **9**, 1736 (2007).

[50] J. L. Rendon and C. J. Serna, Clay Miner. **16**, 375 (1981).

[51] By taking the experimental frequencies of these two phonons for each sample, we can determine the weighted contribution of each based on the value of ν determined from our fitting. Doing so reveals that the weight shifts towards the lower frequency mode with the reduction of size (Figure 3 d).

[52] L. Lu, L. Li, X. Wang, and G. Li, J. Phys. Chem. B **109**, 17151 (2005).

[53] It is well known that electronic transitions can influence phonon behavior, such as resonant Raman, Fano lineshapes, or the Huang-Rhys factor in photoluminescence [54–56]. A good example is electron-molecular vibrational coupling in charge transfer salts, where the temperature dependent vibronic coupling constant directly affects the phonon oscillator strength [57–59]. Other examples of phonon mixing with d- and f-manifold crystal field excitations manifest as avoided crossings [60, 61].

[54] G. Stock and W. Domcke, J. Chem. Phys. **93**, 5496 (1990).

[55] U. Fano, Phys. Rev. **124**, 1866 (1961).

[56] K. Huang and A. Rhys, Proc. R. Soc. Lond. **A204**, 406 (1950).

[57] M. J. Rice, Phys. Rev. Lett. **37**, 36 (1976).

[58] M. J. Rice, V. M. Yartsev, and C. S. Jacobsen, Phys. Rev. B **21**, 3437 (1980).

[59] A. Graja, P. V. Huong, and J. C. Cornut, Solid State Commun. **46**, 8777 (1981).

[60] T.V. Brinzari, J. T. Haraldsen, P. Chen, Q.-C. Sun, Y. Kim, L.-C. Tung, A. P. Litvinchuk, J. A. Schlueter, D. Smirnov, J. L. Manson, J. Singleton, and J. L. Musfeldt, Phys. Rev. Lett. **111** 047202 (2013).

[61] K. N. Boldyrev, T. N. Stanislavchuk, A. A. Sirenko, L. N. Bezmaternykh, and M. N. Popova, Submitted to Phys. Rev. Lett.